Friction **11**(2): 316–332 (2023)
https://doi.org/10.1007/s40544-022-0610-0
ISSN 2223-7690
CN 10-1237/TH
RESEARCH ARTICLE

Molecules with a TEMPO-based head group as high-performance organic friction modifiers

Jinchi HOU[1], Masaki TSUKAMOTO[1], Seanghai HOR[1], Xingyu CHEN[1], Juntao YANG[1], Hedong ZHANG[1,*], Nobuaki KOGA[1], Koji YASUDA[2], Kenji FUKUZAWA[3], Shintaro ITOH[3], Naoki AZUMA[3]

[1] *Department of Complex Systems Science, Graduate School of Informatics, Nagoya University, Nagoya 464-8601, Japan*

[2] *Institute of Materials and Systems for Sustainability, Nagoya University, Nagoya 464-8601, Japan*

[3] *Department of Micro-Nano Systems Engineering, Graduate School of Engineering, Nagoya University, Nagoya 464-8603, Japan*

Received: 25 November 2021 / Revised: 18 January 2022 / Accepted: 19 February 2022

Abstract: High-performance organic friction modifiers (OFMs) added to lubricating oils are crucial for reducing energy loss and carbon footprint. To establish a new class of OFMs, we measured the friction and wear properties of N-(2,2,6,6-tetramethyl-1-oxyl-4-piperidinyl)dodecaneamide referred to as C_{12}Amide-TEMPO. The effect of its head group chemistry, which is characterized by a rigid six-membered ring sandwiched by an amide group and a terminal free oxygen radical, was also investigated with both experiments and quantum mechanical (QM) calculations. The measurement results show that C_{12}Amide-TEMPO outperforms the conventional OFMs of glyceryl monooleate (GMO) and stearic acid, particularly for load-carrying capacity, wear reduction, and stability of friction over time. The friction and wear reduction effect of C_{12}Amide-TEMPO is also greatly superior to those of C_{12}Ester-TEMPO and C_{12}Amino-TEMPO, in which ester and amino groups replace the amide group, highlighting the critical role of the amide group. The QM calculation results suggest that, in contrast to C_{12}Ester-TEMPO, C_{12}Amino-TEMPO, and the conventional OFMs of GMO and stearic acid, C_{12}Amide-TEMPO can form effective boundary films on iron oxide surfaces with a unique double-layer structure: a strong surface adsorption layer owing to the chemical interactions of the amide oxygen and free radical with iron oxide surfaces, and an upper layer owing to the interlayer hydrogen-bonding between the amide hydrogen and free radical or between the amide hydrogen and oxygen. Moreover, the intralayer hydrogen-bonding in each of the two layers is also possible. We suggest that in addition to strong surface adsorption, the interlayer and intralayer hydrogen-bonding also increases the strength of the boundary films by enhancing the cohesion strength, thereby resulting in the high tribological performance of C_{12}Amide-TEMPO. The findings in this study are expected to provide new hints for the optimal molecular design of OFMs.

Keywords: organic friction modifiers (OFMs); TEMPO; friction and wear; surface adsorption; molecular reactivity; boundary lubrication

1 Introduction

Friction and wear at moving parts of machines are estimated to consume 23% of the total energy of the world [1]. Therefore, reducing friction and wear to the lowest possible level is crucial for reducing energy loss and carbon footprint. One cost-effective solution is to use lubricating oils of low viscosity with a small amount of friction modifier additives [2, 3]. Low viscosity is desirable because it leads to low shear resistance between rubbing surfaces intermediated with lubricating oils in the hydrodynamic lubrication regime [2, 4, 5]. As the sliding velocity decreases or the normal load increases, however, low-viscosity oils

* Corresponding author: Hedong ZHANG, E-mail: zhang@i.nagoya-u.ac.jp

are difficult to intervene between rubbing surfaces, causing an undesirable shift from the hydrodynamic to boundary lubrication regime. In the boundary lubrication regime, direct solid–solid contacts are likely to occur, thereby resulting in high friction, severe wear, or even catastrophic system failure. This problem can be solved by the addition of friction modifiers which form boundary films on the rubbing surfaces, and thus prevent direct solid–solid contacts [2, 3, 6–10]. Friction modifier additives not only directly improve the boundary lubrication performance, but also allow the use of low-viscosity lubricating oils, and thus indirectly improve the hydrodynamic lubrication performance. Due to the urgent need for environmental protection, there is an increasing demand for shifting from the currently used sulfur and/or phosphorus-containing additives toward ashless organic friction modifier (OFM) additives that are exclusively composed of carbon, hydrogen, oxygen, and nitrogen atoms [2, 3, 11–14]. Although OFMs have been extensively studied dating back over a century [15, 16], further improvement of the friction and wear reducing performance still remains challenging.

OFMs are usually amphiphiles with a nonpolar hydrocarbon tail group attached to a polar head group [2, 3, 17]. It is generally accepted that OFMs form boundary films with the polar head group adsorbed on solid surfaces and the nonpolar tail group aligned outward into the base oil [2, 18–21]. The design of the head group, which determines the surface adsorption ability of OFMs, and thus load-carrying capacity and durability of the boundary films, is a key issue to improve the performance of OFMs [2, 22–24]. The design factors include the number and type of functional groups in the head group. For the OFMs developed so far, single or multiple functional groups of carboxyl, alcohol, amine, amide, imide, and ester have been used [2, 3, 25–39]. Studies showed that carboxyl and amine groups generally work better than alcohol, ester, and nitrile groups [2, 25]. For instance, Onumata et al. [26] reported that oleic acid exhibited higher effect of friction reduction than oleyl alcohol at steel–steel contacts. Cyriac et al. [27] found that stearamine required less time to form adsorption films on steel surfaces and exhibited lower friction coefficients than OFMs based on amide and carboxyl groups. Fry et al. [28] also showed that octadecylamine exhibited good friction-reducing performance, particularly at the initial stage.

Compared with a single functional group, multiple functional groups can enhance the adsorption strength through multi-site adsorption or chelate effect. Although it has long been considered that multiple functional groups might lower the packing density of the adsorbed molecules due to the relatively large size of the head group [2], recent studies suggested that complete surface coverage was neither practically achievable nor necessary for effective friction reduction [28, 40]. Glyceryl monooleate (GMO), which contains two alcohol groups and one ester group and is one of the most widely employed OFMs [24], was found to give lower friction and wear on steel surfaces than OFMs with a single carboxyl or amine groups [29]. It was also reported that GMO exhibited ultralow friction for rubbing surfaces of tetrahedral amorphous diamond-like carbon (DLC) [2, 30]. Kuwahara et al. [31] found that glycerol, which contained three alcohol groups, also led to ultralow friction with negligible wear on DLC surfaces. Nalam et al. [33] studied the effect of fatty amines with multiple amine groups and found that the adsorbed masses increased with the number of amine groups, while the adsorption kinetics decreased. Hu et al. [34] synthesized a series of OFMs with multiple amine groups and suggested the number of nitrogen atoms and the slim molecular configuration as the main factors affecting the tribological properties. Desanker et al. [36, 37] developed a new type of OFM containing a nitrogen heterocycle with four nitrogen centers and demonstrated its excellent performance in friction and wear reduction. For this new type of OFM, He et al. [38] reported that the increased surface adsorption energy owing to the chelate effect was an essential reason for the increased stability and durability of the surface adsorbed films and thus the excellent boundary lubrication performance, as compared with OFMs with a single amine group.

In contrast, we have proposed N-(2,2,6,6-tetramethyl-1-oxyl-4-piperidinyl)dodecaneamide, which is referred to as C_{12}Amide-TEMPO, as a new class of OFM in our previous study [25]. Its head group is characterized by a rigid six-membered ring with a free radical at

the terminal and an amide group at the opposite side, as seen from Fig. 1(a). Although TEMPO (i.e., the six-membered ring with a free radical) and its derivatives with a hydroxy, oxo, or carboxamido group at the 4 position have been reported as high-performance antiwear and antioxidant additives [41], it was the first trial to use molecules with TEMPO attached to an alkyl chain via an amide linkage as an OFM. We suppose that the free radical and amide group provide strong surface adsorption and the rigid ring helps to carry normal loads. Pin-on-disk type tribological tests demonstrated that C_{12}Amide-TEMPO exhibited higher load-carrying capacity and more stable sliding than stearic acid [25].

In this study, besides friction properties, the antiwear performance of C_{12}Amide-TEMPO was measured. GMO was included as a benchmark in addition to stearic acid which is a model OFM highly effective in friction reduction but causing metal corrosion [42]. Moreover, to understand the effect of the head group chemistry, we compared C_{12}Amide-TEMPO with C_{12}Ester-TEMPO and C_{12}Amino-TEMPO, in which ester and amino linkages replace the amide linkage in C_{12}Amide-TEMPO, as illustrated in Figs. 1(b) and 1(c). The comparison included experimentally measured friction properties and theoretically calculated molecular reactivity and surface adsorption properties. Based on the experimental and calculation results, we proposed a model of double-layer adsorption for C_{12}Amide-TEMPO, which is unique and is probably one reason for the superior tribological performance of C_{12}Amide-TEMPO as compared with the other OFMs used in this study.

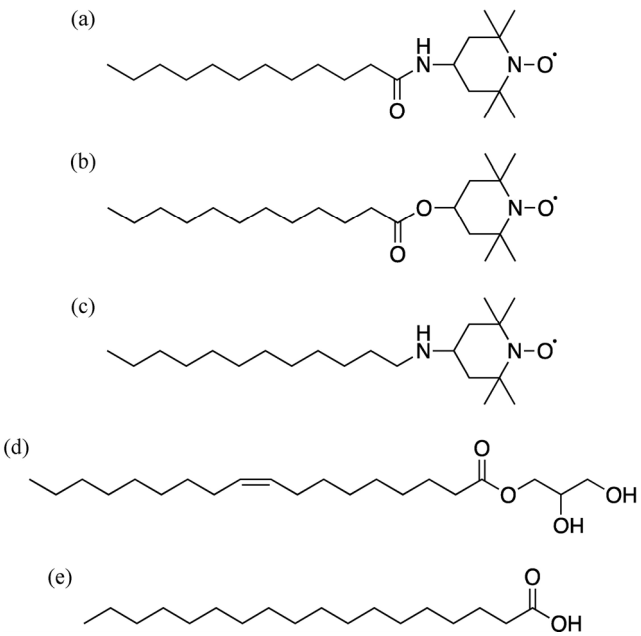

Fig. 1 Chemical structures of the OFMs used in this study: (a) C_{12}Amide-TEMPO, (b) C_{12}Ester-TEMPO, (c) C_{12}Amino-TEMPO, (d) GMO, and (e) stearic acid.

2 Materials and methods

2.1 Lubricants

As described in Section 1, C_{12}Amide-TEMPO, C_{12}Ester-TEMPO, C_{12}Amino-TEMPO, GMO, and stearic acid were used as OFMs in this study. Their chemical structures are illustrated in Fig. 1, and their molecular weights are 353.57, 354.55, 339.58, 356.54, and 284.48 g/mol, respectively. A hexane solution (100 mg/mL) of GMO, (purity: 99%) was obtained from Olbracht Serdary Research Laboratories and used after removing hexane. Stearic acid (purity: > 98.0% (T)) was obtained from Tokyo Chemical Industry and used as received. C_{12}Amide-TEMPO and C_{12}Amino-TEMPO were synthesized by the reported methods [43, 44]. C_{12}Ester-TEMPO was synthesized by a slight modification of the reported method as follows [45]. A solution of dodecanoyl chloride (2.1 mL, 8.8 mmol) in tetrahydrofuran (10 mL) was slowly added to a cool (0 °C) solution of 4-hydroxy-TEMPO (1.7 g, 9.9 mmol) and triethylamine (4.2 mL, 30 mmol) in tetrahydrofuran (10 mL) under Ar atmosphere. The reaction mixture was stirred for 21 h at 30 °C. After removing the tetrahydrofuran under the reduced pressure, the residue was dissolved in EtOAc (100 mL) and washed with saturated $NaHCO_3$ (aq, 100 mL). The aqueous phase was back-extracted with EtOAc (100 mL × 2), and the combined organic phase was dried over Na_2SO_4, evaporated, and dried under reduced pressure to give a crude product, which was purified by the normal-phase medium-pressure liquid chromatography (the ratio of hexane:EtOAc is from 97:3 to 76:24) to afford C_{12}Ester-TEMPO (2.5 g, 80%): LRMS (EI) calcd for $C_{21}H_{40}NO_3$ $[M]^{+\bullet}$ 354, found 354. At room temperature, C_{12}Amide-TEMPO is a pink-colored powder, and C_{12}Ester-TEMPO and C_{12}Amino-TEMPO are red-orange oils.

The base oil used was synthetic oil poly-alpha-olefin (PAO) with the viscosity of 30.3 cSt at 40 °C and 5.79 cSt at 100 °C. Each OFM was dissolved in PAO by stirring for approximately 30 min at the temperature of 65 °C. The concentration was determined to be 0.5 wt% based on the friction reduction performance of 0.1, 0.5, 1.0 wt% C_{12}Amide-TEMPO solutions (Fig. S1 in the Electronic Supplementary Material (ESM)). All the solutions were clear at the temperature of 40 °C used for tribological tests.

To investigate the effect of the free radical in the TEMPO-type OFMs, we synthesized compounds by replacing the oxygen radical with hydrogen (H–), methyl group (CH_3–), or acetyl group (CH_3CO–). We also tried to use commercially available stearamide [$CH_3(CH_2)_{16}CONH_2$], which has the alkyl chain and amide group but not the TEMPO group as compared with C_{12}Amide-TEMPO. However, these compounds were not used for tribological tests because they are not soluble in PAO at the concentration of 0.5 wt%.

2.2 Tribological tests

The pin-on-disk type unidirectional tribotester illustrated in Fig. 2 was used for tribological tests. The sliding pins were balls of 8 mm in diameter, and the disks were square plates of 30 mm in length and width and 1 mm in thickness. Both the pins and disks were made of SUS304 stainless steel. The pins and disks were purchased and used after rinsed with hexane for 5 min. The surface roughness was measured by the atomic force microscope (Dimension Icon, Bruker AXS) using three pins and three disks. The measurement area was 20.0 μm × 20.0 μm. The average values of the arithmetic mean roughness (R_a) and root-mean-square roughness (R_q) were 15.1 and 21.4 nm for the pins, and 0.76 and 1.33 nm for the disks [25].

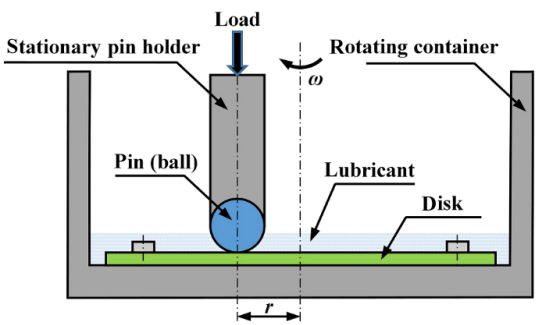

Fig. 2 Schematic illustration of the pin-on-disk type tribotester.

In this study, 2 mL lubricants were filled in the container of the tribotester, flooding the gap between the pin and disk. The temperature of the lubricants was kept constant at 40 °C with a heater embedded under the oil container. The sliding radius and rotational speed (r and ω in Fig. 2) were fixed at 6.5 mm and 30 r/min, respectively, giving rise to a sliding velocity of 20.4 mm/s. Two types of tribological tests were performed. One type was to assess the load-carrying capacity of the OFMs by increasing the normal load from 1.0 to the limit of 43.7 N of the tribotester (i.e., mean Hertzian contact pressure of 0.35–1.23 GPa). At each normal load, sliding was performed for 5 min, and the frictional forces measured in the last 3 min were averaged as the final result. The tests with the increased normal loads were continuously conducted at the same sliding track. The other type was to assess the stability of friction and antiwear performance of the OFMs with sliding at a fixed normal load for 1 h. During sliding, the change of frictional force was measured with time, and after sliding, the wear of the pin and disk was measured with a laser microscope (LEXT OLS5000, Olympus). The normal load was set to be 5.0, 29.2, or 43.7 N (i.e., mean Hertzian contact pressure of 0.60, 1.08, or 1.23 GPa), and the new pin and disk were used for each normal load. The minimum film thickness h_{min} and the dimensionless lambda ratio Λ were calculated using Eqs. (1) and (2), respectively [46, 47].

$$h_{\min} = 3.63R\left(\frac{\eta_0 u}{E'R}\right)^{0.68}(\alpha E')^{0.49}\left(\frac{F}{E'R^2}\right)^{-0.0.73}(1-\mathrm{e}^{-0.68k}) \tag{1}$$

$$\Lambda = \frac{h_{\min}}{\sqrt{R_{qp}^2 + R_{qd}^2}} \tag{2}$$

where R is the radius of the sliding pin, η_0 is the lubricant viscosity at the atmospheric pressure, u is the mean sliding velocity of the pin and disk, E' is the reduced Young's modulus, α is the pressure–viscosity coefficient, F is the normal load, k is a contact ellipticity parameter (equal to 1 in this study), and R_{qp} and R_{qd} are the root-mean-square roughnesses of the pin and disk, respectively. With the normal loads

and sliding velocity used in this study, η_0 = 23.9 mPa·s, E' = 218.4 GPa, and α = 13.5 GPa^{-1} [25], h_{min} and Λ were calculated to be no larger than 3.94 nm and 0.18, respectively, showing that all the tests were conducted in the boundary lubrication regime.

2.3 Quantum mechanical calculations

To gain insight into the influence of the molecular structure of TEMPO-type OFMs, we carried out two types of Quantum mechanical (QM) calculations using density functional theory (DFT). First, molecular geometries were optimized, and electrostatic potentials (ESPs) were calculated using the Gaussian 16 package [48], in order to understand the molecular reactivity. The M06-2X hybrid functional [49] was used in conjunction with the 6-31G(d) basis set [50–52]. Frequency calculations at the same level were performed to ensure that the optimized results corresponded to energy minima.

Then, DFT calculations of TEMPO-type OFMs on iron oxide surfaces were carried out using the Vienna *ab initio* Simulation Package (VASP) with the projector augmented wave (PAW) method, in order to identify the most stable adsorbed structures and quantify the adsorption energies. Following Ref. [53], α-Fe_2O_3 (0001) was used as the iron oxide surfaces and modeled as a single Fe-terminated 6-layer slab 10.07 Å × 15.105 Å (i.e., 2 × 3 hexagonal supercell) in length and width. Each Fe bilayer is ferromagnetic, and adjacent bilayers are coupled antiferromagnetically [53, 54]. Electronic correlations in the Fe 3d orbitals were accounted for by adding a Hubbard $U - J$ = 4eV (in the Dudarev approach [53, 55]). This results in an indirect band gap of 1.71 eV, which is within the experimentally observed range (1.38–2.09 eV [56]). Because the adsorption of OFMs on the solid surfaces is mostly determined by the strong Coulomb interaction of the functional groups rather than the weak van der Waals interaction of the alkyl chain, C_3Amide-TEMPO, C_3Ester-TEMPO, and C_3Amino-TEMPO were used to reduce the calculation time. The surface coverage of these OFM molecules was 0.75 molecule/nm^2, sufficiently low to avoid intermolecular interactions. The iron oxide surface and OFM molecules were first geometrically optimized separately, and then the complexes of each of the OFM molecules on the iron oxide surface were geometrically optimized. Periodic boundary conditions were applied to the in-plane directions, while a vacuum layer at least 15 Å thick was set in the out-of-plane direction to prevent interactions between the neighboring cells. The adsorption energy E_{ad} was calculated as

$$E_{ad} = E_{sys} - E_{sub} - E_{mol} \quad (3)$$

where E_{sys}, E_{sub}, and E_{mol} are the total energies of the optimized complex, solid substrate, and OFM molecule, respectively. Also following Ref. [57], the optB86b-vdW functional was used to include van der Waals interactions, and all calculations were spin-polarized. The plane-wave cutoff was set to 550 eV, and a Monkhorst–Pack *k*-point mesh of 4 × 4 × 2 was used. A dipole correction was also applied.

3 Results

3.1 Comparison of C_{12}Amide-TEMPO, GMO, and stearic acid

3.1.1 *Load-carrying capacity and stability of friction*

First, the load-carrying capacity of C_{12}Amide-TEMPO, GMO, and stearic acid was compared from the change in the friction coefficient with increasing normal load (Fig. 3). The friction coefficient of C_{12}Amide-TEMPO

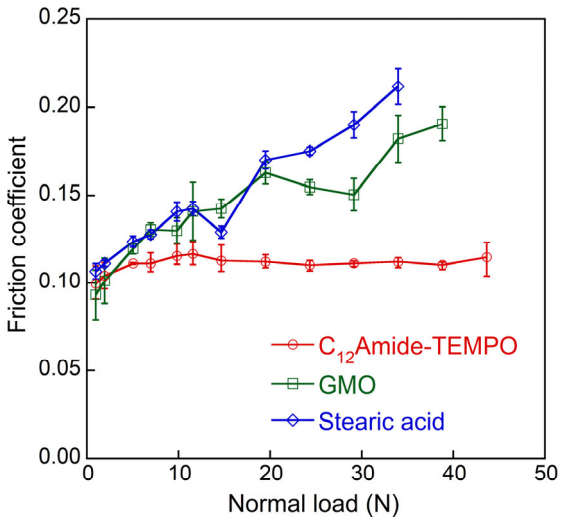

Fig. 3 Changes in the friction coefficient with increasing normal load for C_{12}Amide-TEMPO, GMO, and stearic acid. The error bars indicate the maximum and minimum of three independent experiments.

remains at a low level even under high loads, whereas the friction coefficients of GMO and stearic acid increase obviously with load. The three OFMs are roughly equally effective in friction reduction under loads less than 5 N; however, beyond that load, C_{12}Amide-TEMPO is evidently more effective than GMO and stearic acid. The friction coefficient of GMO is comparable to that of stearic acid under loads less than 20 N, whereas beyond that load, the former is lower than the latter. These results demonstrate that the load-carrying capacity ranks in the order: C_{12}Amide-TEMPO >> GMO > stearic acid. Although the load-carrying capacity of C_{12}Amide-TEMPO is yet to be determined due to the constraint of the upper load of the tribotester, we can conclude from Fig. 3 that it is larger than 1.2 GPa in terms of mean Hertzian contact pressure or 1.8 GPa in terms of maximum Hertzian contact pressure.

Then, the stability of friction was compared for C_{12}Amide-TEMPO, GMO, and stearic acid from the time evolution of the friction coefficient during 1-h sliding tests (Fig. 4). The normal load was 5.0, 29.2, and 43.7 N (i.e., mean Hertzian contact pressure of 0.6, 1.1, and 1.2 GPa) for C_{12}Amide-TEMPO, but the highest load of 43.7 N was not applied to GMO and stearic acid because they are ineffective at this load as confirmed from Fig. 3. Table 1 shows the time-averaged friction coefficient of the 1-h sliding tests. Aside from the time-averaged values, it is noteworthy from Fig. 4 that in contrast to the large fluctuation in the friction coefficient observed for GMO and stearic acid, C_{12}Amide-TEMPO exhibits stable low friction during the 1-h sliding tests. The fluctuation of the friction coefficient of GMO is comparable to that of stearic acid at the relatively low load of 5.0 N, whereas it is smaller than that of stearic acid when the load increases to 29.2 N. These results demonstrate that the stability of friction ranks in the order: C_{12}Amide-TEMPO >> GMO > stearic acid, which is consistent with the rank of load-carrying capacity. Note that the friction coefficient of C_{12}Amide-TEMPO was relatively large and unstable initially, and it decreased to a stable low value with time. When the disks were treated with oxygen plasma for 1 min, the friction coefficient in the initial period decreased to some extent, whereas the steady-state friction coefficient remained roughly unchanged (Fig. S2 in the ESM). These results are consistent with Ref. [58], indicating that surface cleaning procedures largely affect the friction coefficients at the initial state rather than at the steady state. Therefore, for easy sample preparation, all the disks and pins were not treated with oxygen plasma and were only rinsed with hexane for 5 min in this study.

3.1.2 *Antiwear performance*

Finally, the antiwear performance of C_{12}Amide-TEMPO, GMO, and stearic acid was compared. From the topography of the wear scar on the disk and pin after the 1-h sliding tests, wear was observed for all the disks (Fig. 5), whereas accumulation was more frequently observed than wear for the pins (Fig. S3 in

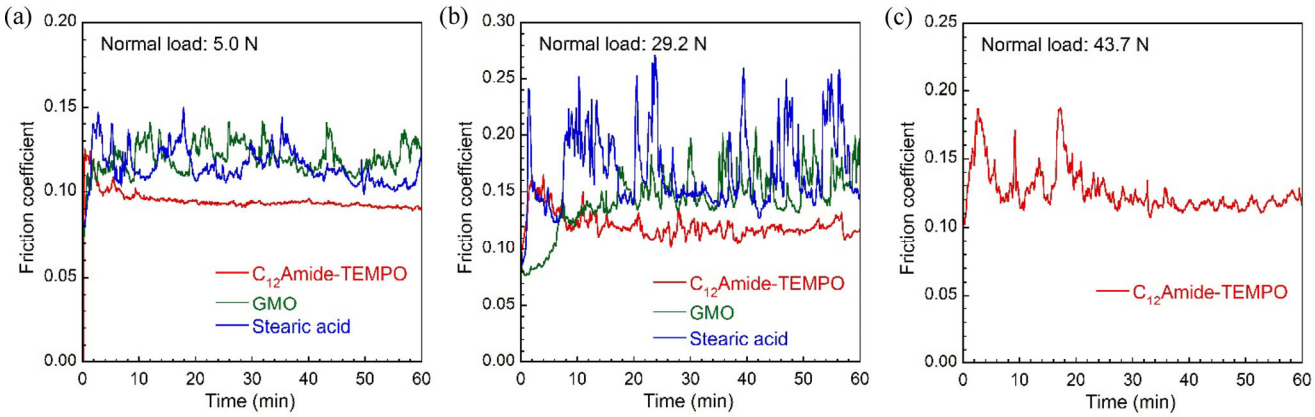

Fig. 4 Time evolution of the friction coefficient for C_{12}Amide-TEMPO, GMO, and stearic acid during 1-h sliding tests. The normal load was (a) 5.0, (b) 29.2, and (c) 43.7 N, but the largest load of 43.7 N was not applied to GMO and stearic acid. Note that the scales of the vertical axes in (a) and (c) are different from that in (b).

Table 1 Time-averaged friction coefficient of C_{12}Amide-TEMPO, GMO, and stearic acid at different normal loads during 1-h sliding tests.

OFM	Averaged friction coefficient		
	5.0 N	29.2 N	43.7 N
C_{12}Amide-TEMPO	0.095	0.12	0.13
GMO	0.12	0.15	—
Stearic acid	0.12	0.17	—
C_{12}Ester-TEMPO	0.20	—	—
C_{12}Amino-TEMPO	0.20	—	—

the ESM). Therefore, as will be described below, we analyzed only the data for wear of disk to quantitively assess the antiwear performance.

For direct visual comparison, the cross-sectional profiles along the horizontal dashed lines in Fig. 5 are shown in Fig. 6. It is evident that among the three OFMs, C_{12}Amide-TEMPO exhibits the best antiwear performance, giving rise to the narrowest, shallowest, and smoothest wear tracks. This is consistent with the literature showing that the addition of TEMPO and TEMPO derivatives can largely improve the antiwear performance of lubricating oils [41]. Figure 7 quantitatively compares the wear track width, specific wear rate, and area-based surface roughness (*Sa*) of the three OFMs. For reference, the wear volumes on the sliding pins are shown in Fig. S4 in the ESM. Here the specific wear rate was calculated with

$$\text{Specific wear rate} = \frac{\text{Wear volume } (\mu m^3)}{\text{Normal load (N)} \times \text{Sliding distance (mm)}} \quad (4)$$

The wear track widths and surface roughnesses of the three OFMs and the specific wear rates of C_{12}Amide-TEMPO and stearic acid increase with the increasing normal load, whereas the specific wear rate of GMO decreases slightly with the increasing normal load. Compared with GMO and stearic acid, C_{12}Amide-TEMPO reduces the wear track width by 37% and 27%, the specific wear rate by 70% and 63%,

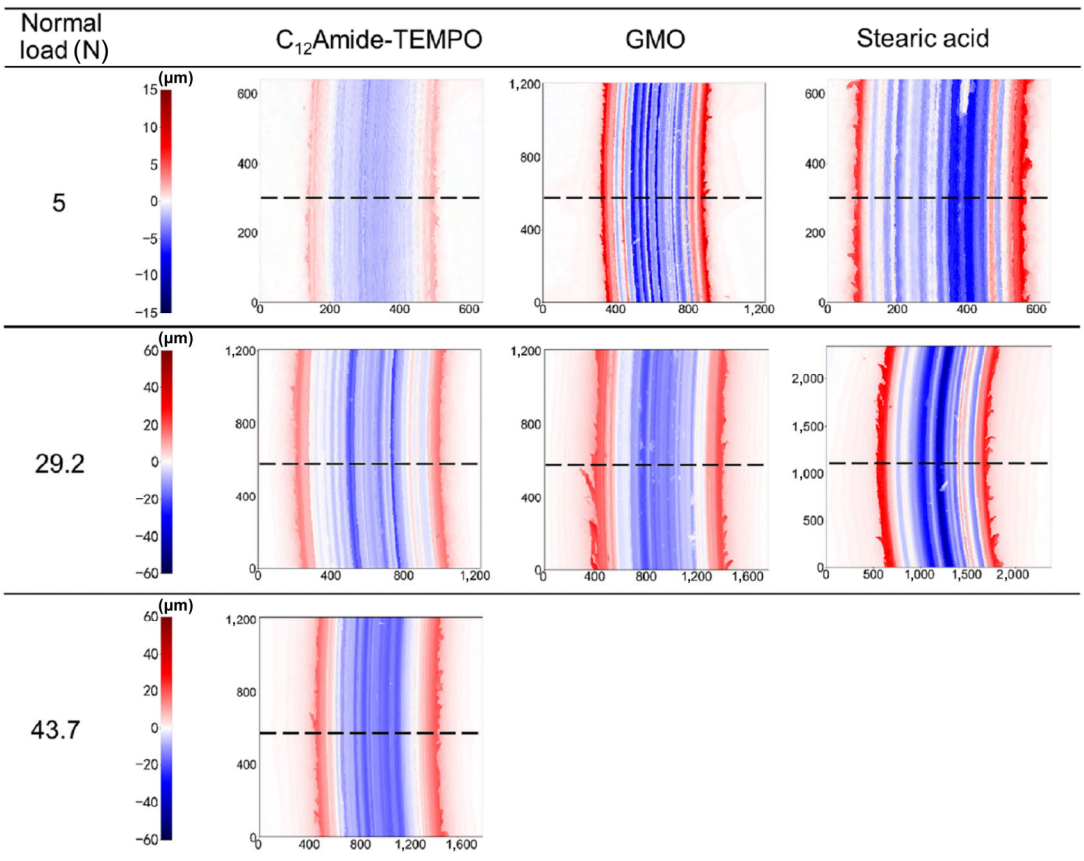

Fig. 5 Surface topography of the wear scar on the disk. Red and blue colors indicate accumulation and wear, respectively. Note that the color scale and the length and width (unit: μm) of the measured area are different for all the images.

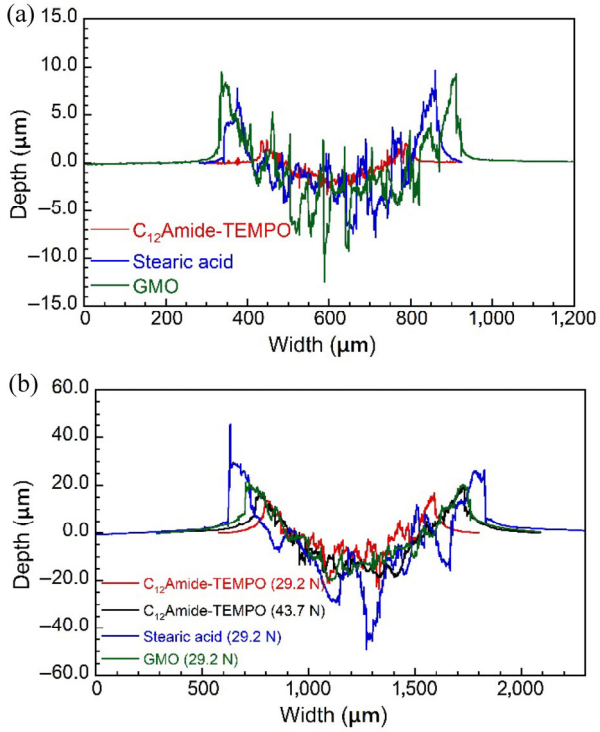

Fig. 6 Cross-sectional profile of the wear track on the disk along the horizontal dashed line in Fig. 5. The normal load was (a) 5.0 N, (b) 29.2 and 43.7 N (for C_{12}Amide-TEMPO only). Note that the axis scales of (a) and (b) are different.

and the surface roughness by 62% and 70% at the normal load of 5.0 N. At the normal load of 29.2 N, the reduction rates by C_{12}Amide-TEMPO as compared with GMO and stearic acid are 24% and 30% for the wear track, 39% and 65% for the specific wear rate, and 32% and 49% for the surface roughness. The wear track width, specific wear rate, and surface roughness for C_{12}Amide-TEMPO at the normal load of 43.7 N are even 5%, 30%, and 3% less than those for GMO at the normal load of 29.2 N and 13%, 59%, and 26% less than those for stearic acid at the normal load of 29.2 N. From Table 1, we know that compared with GMO and stearic acid, C_{12}Amide-TEMPO reduces the friction coefficient by both 21% at the normal load of 5.0 N and by 20% and 29% at the normal load of 29.2 N. The reduction rate of the specific wear rate and surface roughness by C_{12}Amide-TEMPO is 1.6–3.4 times larger than those of the friction coefficients at the normal loads of 5.0 and 29.2 N. Hence, we suggest that the excellent antiwear performance of C_{12}Amide-TEMPO may be associated not only with the small time-averaged friction coefficient but also

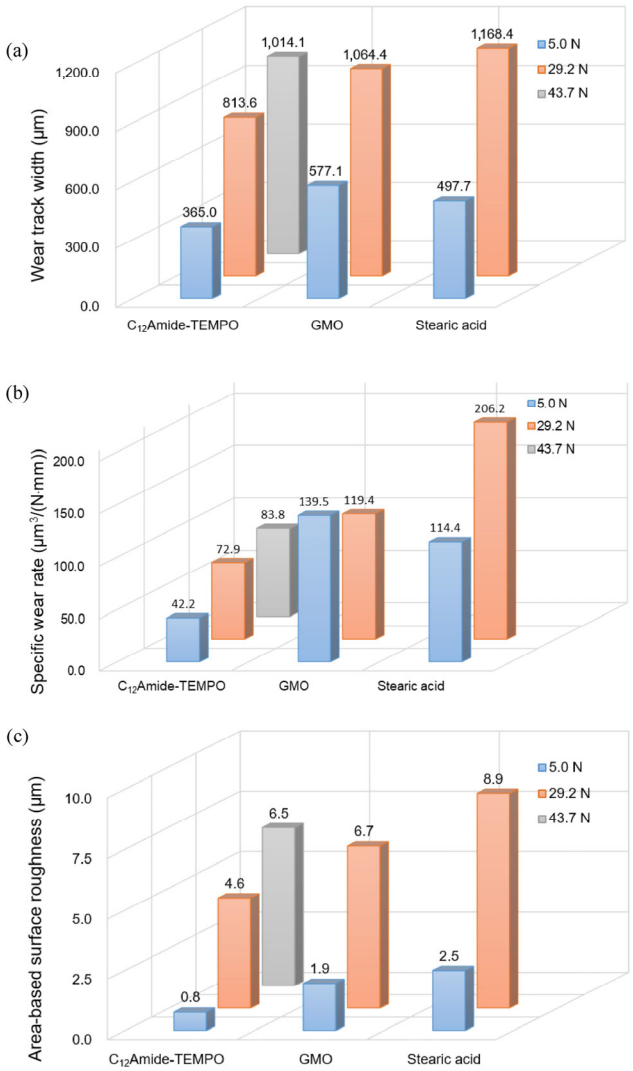

Fig. 7 (a) Wear track widths, (b) specific wear rates, and (c) area-based surface roughnesses on the disks.

with the small fluctuation over time (i.e., the high stability of friction).

3.2 Comparison of C_{12}Amide-TEMPO, C_{12}Ester-TEMPO, and C_{12}Amino-TEMPO

3.2.1 *Friction and wear reduction performance*

The friction-reduction performances of C_{12}Amide-TEMPO, C_{12}Ester-TEMPO, C_{12}Amino-TEMPO were compared in term of the time evolution of the friction coefficient during 1-h sliding tests (Fig. 8). In contrast to the low and stable friction of the former, the latter two show high and fluctuating friction even though the normal load was as small as 5.0 N. The topography of wear scars and the cross-sectional profiles of the

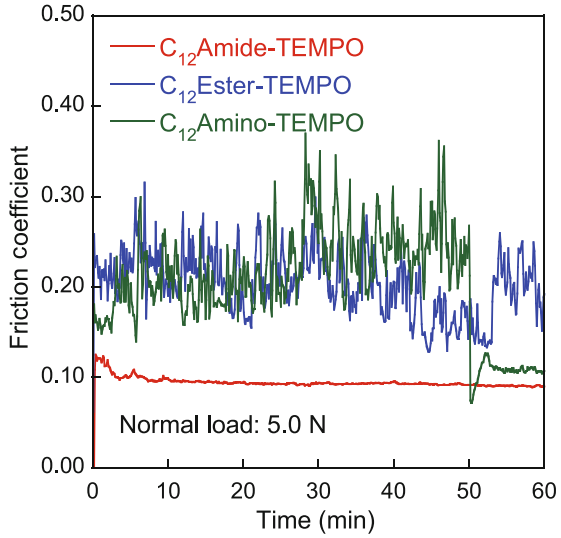

Fig. 8 Time evolution of the friction coefficients for C_{12}Amide-TEMPO, C_{12}Ester-TEMPO, and C_{12}Amino-TEMPO during 1-h sliding tests.

wear tracks on the disks for the three TEMPO-based OFMs are shown in Figs. S5 and S6 in the ESM. For C_{12}Ester-TEMPO and C_{12}Amino-TEMPO, the wear track widths are 569.0 and 544.0 μm, respectively, and the specific wear rates are 461.2 and 196.9 $\mu m^3/(N \cdot mm)$, respectively, all considerably larger than the values (365.0 μm and 42.2 $\mu m^3/(N \cdot mm)$) for C_{12}Amide-TEMPO. The friction and wear reduction performance of C_{12}Ester-TEMPO and C_{12}Amino-TEMPO is even poor as compared with GMO and stearic acid (Fig. 4(a), Table 1, and Figs. 7(a) and 7(b)). These results demonstrate that the amide group in C_{12}Amide-TEMPO is crucial for the observed good tribological performance. The underlying mechanism for the contribution of the amide group and the reason for the poor friction-reduction performance of C_{12}Ester-TEMPO and C_{12}Amino-TEMPO will be discussed in Section 4.

3.2.2 *Molecular reactivity*

Figure 9 illustrates the molecular ESPs on the 0.001 a.u. electron density isosurface of geometrically optimized C_{12}Amide-TEMPO, C_{12}Ester-TEMPO, and C_{12}Amino-TEMPO. The positions and values of minima and maxima of the ESP were analyzed using the Multiwfn program [59, 60] and indicted in Fig. 9. A common feature of the three TEMPO-type molecules is that a large area of strongly negative ESP and two

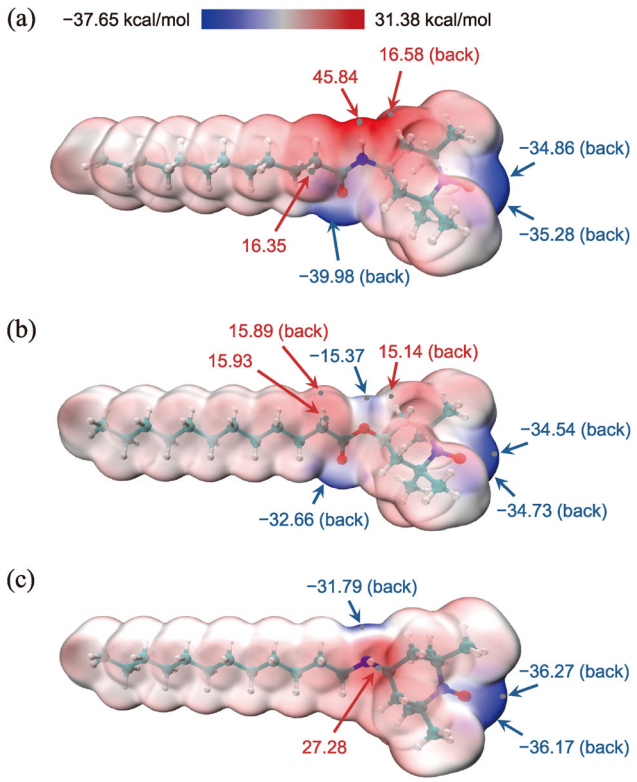

Fig. 9 Molecular ESPs on the 0.001 a.u. electron density isosurface of geometrically optimized (a) C_{12}Amide-TEMPO, (b) C_{12}Ester-TEMPO, and (c) C_{12}Amino-TEMPO. Positive and negative ESP regions are indicated in red and blue colors, respectively. Positions and values of the local minimum and maximum ESPs with absolute values larger than 15.00 kcal/mol are also indicated with blue and yellow points and numbers. Figures were rendered using Visual Molecular Dynamics (VMD) [61].

minima with roughly equal values are located near the oxygen radical (O•). These minima are the global minima for C_{12}Ester-TEMPO and C_{12}Amino-TEMPO, whereas the global minimum is associated with the amide oxygen (O_{amide}) for C_{12}Amide-TEMPO. The ester oxygen (O_{ester}) in C_{12}Ester-TEMPO and the amino nitrogen (N_{amino}) in C_{12}Amino-TEMPO also exhibit strongly negative ESP values, but are weaker than those of O• and O_{amide}. Another distinct feature of C_{12}Amide-TEMPO is that the amide hydrogen (H_{amide}) exhibits strongly positive ESP of 45.84 kcal/mol, approximately 1.7 times larger than that of amino hydrogen (H_{amino}) in C_{12}Amino-TEMPO. As iron and oxygen atoms of the iron oxide surfaces (Fe_{surf} and O_{surf}) possess positive and negative charges, respectively, surface adsorption of C_{12}Amide-TEMPO can occur via three different interactions: O•–Fe_{surf}, O_{amide}–Fe_{surf},

and H_{amide}–O_{surf}. In contrast, there are only two different interactions: O•–Fe_{surf} and O_{ester}–Fe_{surf} in C_{12}Ester-TEMPO and O•–Fe_{surf} and N_{amino}–Fe_{surf} in C_{12}Amino-TEMPO.

3.2.3 *Surface adsorption properties*

Figure 10 shows the most stable adsorbed structure of C_3Amide-TEMPO, C_3Ester-TEMPO, and C_3Amino-TEMPO on the Fe_2O_3 (001) surface. All these molecules lie flat on the surface, thereby maximizing both the number of bonds between the head group and surface and the van der Waals interactions between the alkyl chain and surface. Consistent with the above-described results of molecular ESP, two bonds are developed between the head group and surface: O•–Fe_{surf} and O_{amide}–Fe_{surf} for C_3Amide-TEMPO, O•–Fe_{surf} and O_{ester}–Fe_{surf} for C_3Ester-TEMPO, and O•–Fe_{surf} and N_{amino}–Fe_{surf} for C_3Amino-TEMPO. As noted in Fig. 10, the lengths of these bonds are 1.97–2.13 Å, comparable to the O–Fe bond length (1.94 and 2.09 Å) in bulk hematite [62]. This indicates that the three TEMPO-type OFMs can chemically adsorb on iron oxide surfaces. For C_3Amide-TEMPO, the lengths of O•–Fe_{surf} and O_{amide}–Fe_{surf} are equal, suggesting that the oxygen radical and amide oxygen contribute equally to the chemisorption. In contrast, the length of O•–Fe_{surf} is slightly shorter than those of the other bonds for C_3Ester-TEMPO and C_3Amino-TEMPO, suggesting that the oxygen radical is more responsible for the chemisorption than the ester and amino groups.

The adsorption energies for these most stable structures are shown in Table 2. For comparison, the adsorption energies of hexanoic acid

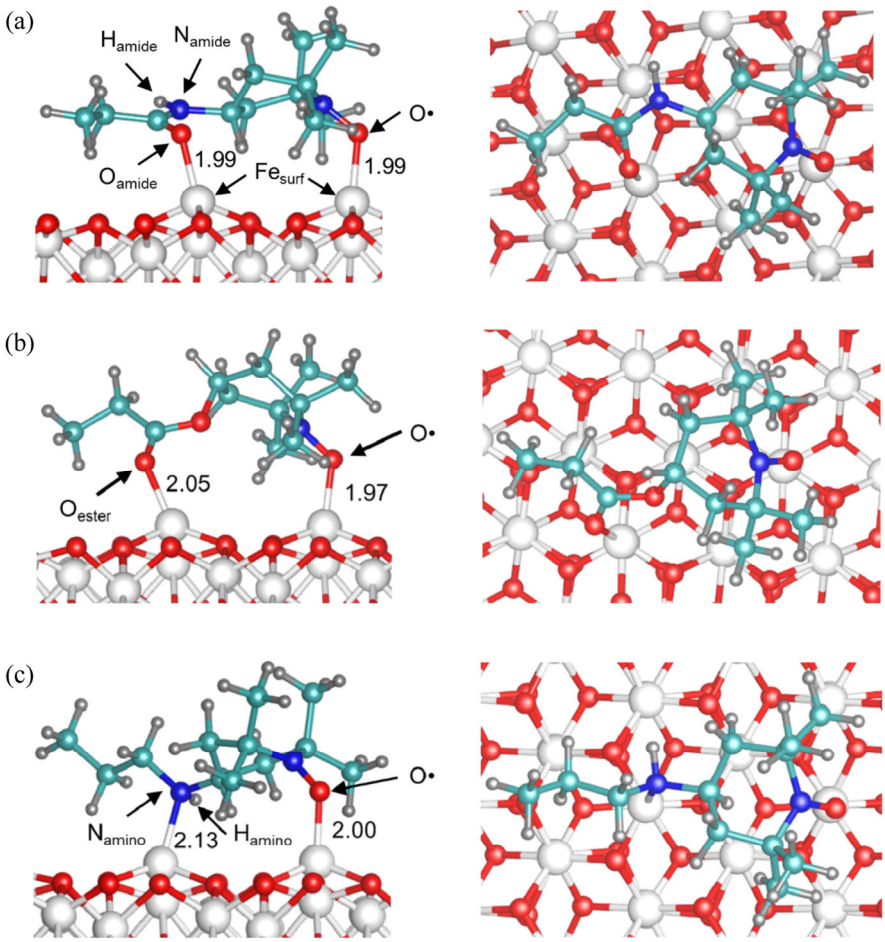

Fig. 10 (left) Front and (right) top views of the most stable adsorbed structure of (a) C_3Amide-TEMPO, (b) C_3Ester-TEMPO, and (c) C_3Amino-TEMPO on the Fe_2O_3 (001) surface. The values indicate the bond distances (unit: Å). White, red, gray, cyan, and blue colors represent iron, oxygen, hydrogen, carbon, and nitrogen atoms, respectively. Figures were rendered using Visualization for Electronic and Structural Analysis (VESTA) [63].

(HA:$CH_3(CH_2)_4COOH$) and glyceryl monohexanate (GMH:$CH_3(CH_2)_4COOCH_2CHOHCH_2OH$) from Ref. [53], which have the same head group as stearic acid and GMO but a shorter alkyl chain, are also presented in Table 2. It should be noted that the negative sign of the adsorption energies indicates attractive interactions, and the absolute value indicates the adsorption strength. C_3Amide-TEMPO shows the strongest adsorption, approximately 1.7 and 1.3 times stronger than those of HA and GMH. It should be noted that besides the structure shown in Fig. 10(a), C_3Amide–TEMPO can also adsorb on the iron oxide surfaces via O•–Fe_{surf} and H_{amide}–O_{surf} with an adsorption energy of −69.6 kcal/mol (Fig. S7 in the ESM). C_3Ester-TEMPO and C_3Amino-TEMPO also exhibit stronger adsorption energies than those of HA and GMH, which however cannot explain their poor friction-reduction effect as compared with stearic acid and GMO. Consequently, we infer that strong surface adsorption is a necessary but not a sufficient condition for good tribological performance of OFMs. Further detailed discussion will be given in Section 4.

Table 2 Adsorption energies calculated with Eq. (3) for the most stable adsorbed structures of different OFMs. The values for hexanoic acid and glyceryl monohexanate are from Ref. [53].

OFM	E_{ad} (kcal/mol)
C_3Amide-TEMPO	−94.1
C_3Ester-TEMPO	−79.1
C_3Amino-TEMPO	−86.0
Hexanoic acid	−54.7
Glyceryl monohexanate	−73.6

4 Discussion

As described in Section 3.1, C_{12}Amide-TEMPO outperforms GMO and stearic acid, particularly for load-carrying capacity, stability of friction over time, and antiwear performance. These experimental results suggest that the C_{12}Amide-TEMPO boundary films are more durable against heavy-loaded and prolonged sliding than the boundary films of GMO and stearic acid. As described in Section 3.2.1, the friction and wear reduction effect of C_{12}Amide-TEMPO is greatly superior to those of C_{12}Ester-TEMPO and C_{12}Amino-TEMPO. Therefore, we suggest that the two functional groups in C_{12}Amide-TEMPO, i.e., the amide and free oxygen radical, are crucial for ensuring the durability of the boundary films. The conceivable reasons are elaborated below.

As illustrated in Fig. 11, we consider that the contribution of the amide group and oxygen radical is three folds. First, the amide oxygen and free radical interact chemically with iron oxide surfaces, thereby forming a strong surface adsorption layer. As suggested by the results in Table 2, C_{12}Amide-TEMPO shows higher adsorption energy on iron oxide surfaces than C_{12}Amino-TEMPO, C_{12}Ester-TEMPO, and the conventional OFMs of GMO and stearic acid. Second, because the amide serves as both hydrogen bond donor and acceptor and the oxygen radical serves as the hydrogen bond acceptor, they help to form a diffusive layer on the adsorbed one as in electric double layers through the interlayer hydrogen-bonding of H_{amide}–O• or H_{amide}–O_{amide}. Note that the interaction energies of the two types of hydrogen-bonding were calculated with VASP to be −11.6 and −10.8 kcal/mol. Third, intralayer hydrogen-bonding can also form in each of the two layers between H_{amide}–O• or H_{amide}–O_{amide}. Such double-layer structure induced by both surface interactions and interlayer and intralayer hydrogen-bonding interactions has not been reported in the literature to our knowledge, and it is difficult to be formed by C_{12}Ester-TEMPO, C_{12}Amino-TEMPO, and the conventional OFMs of GMO and stearic acid, as will be described later. We suggest that in addition to strong surface adsorption, the interlayer and intralayer hydrogen-bonding also increases the strength of the boundary films by enhancing the cohesion strength, thereby rendering the films difficult to be sheared off during heavily-loaded and long-time

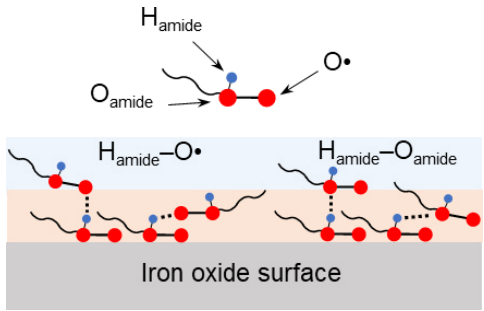

Fig. 11 Adsorption model of C_{12}Amide-TEMPO on iron oxide surfaces.

sliding. Moreover, the upper layer might serve as a buffer to protect the surface adsorption layer, which is the last barrier to prevent solid–solid contacts, against shear. Therefore, we suggest that the good tribological performance of C_{12}Amide-TEMPO, particularly the high load-carrying capacity, high stability of friction, and excellent antiwear performance as compared with GMO and stearic acid, is likely attributed to the unique double-layer structure of the boundary films.

As seen from Fig. 1, stearic acid has only one functional group. GMO has two functional groups; however, it is more energetically stable with both of its functional groups adsorbed on iron oxide surfaces, as indicated by the QM calculations [53]. Consequently, once stearic acid and GMO adsorb on solid surfaces, they are difficult to interact with other molecules, and thereby difficult to form the double-layer structure like C_{12}Amide-TEMPO (Fig. 11). C_{12}Ester-TEMPO and C_{12}Amino-TEMPO are also difficult to form the boundary films with the double-layer structure for the reasons described below. As seen from Fig. 9, C_{12}Ester-TEMPO is difficult to develop intermolecular interaction, whereas the hydrogen-bonding of H_{amino}–O• can be developed between C_{12}Amino-TEMPO molecules. However, when C_{12}Amino-TEMPO molecules adsorb on the surfaces via O• and N_{amino}, they are difficult to interact with other C_{12}Amino-TEMPO molecules via H_{amino}–O•. The reason is as follows. As seen from Fig. 10(c), the bond angle of H_{amino}–N_{amino}–Fe_{surf} is 88.4°. It is much smaller than the bond angle of 109.5° in nitrogen-centered tetrahedral structure, demonstrating that an agnostic-like interaction exists between H_{amino} and Fe_{surf}. Due to this interaction, H_{amino} is pulled close to the iron oxide surface, with its distance from Fe_{surf} being 2.37 Å, and its bond length with N_{amino} being slightly elongated to 1.03 Å as compared with 1.02 Å in the isolated C_3Amino-TEMPO. As a result, H_{amino} is difficult to be approached by O• of other C_{12}Amino-TEMPO molecules, and an upper layer on the surface-adsorbed molecules is difficult to form.

However, the above-described difference is not sufficient to explain the far inferior tribological performance of C_{12}Ester-TEMPO and C_{12}Amino-TEMPO even as compared with GMO and stearic acid. The poor performance even at the low normal load of 5.0 N suggests that C_{12}Ester-TEMPO and C_{12}Amino-TEMPO are difficult to form effective boundary films. Formation of effective boundary films involves two processes for OFMs: first approaching solid surfaces, and then interacting with surface active sites. As C_{12}Ester-TEMPO and C_{12}Amino-TEMPO show larger adsorption energies than GMO and stearic acid (Table 2), we suggest that C_{12}Ester-TEMPO and C_{12}Amino-TEMPO are difficult to approach solid surfaces. The reason probably lies on the low polarity of C_{12}Ester-TEMPO and C_{12}Amino-TEMPO, which renders them highly soluble in the nonpolar base oil of PAO and thus difficult to diffuse and approach to solid surfaces. Previous studies have also demonstrated that OFMs with high solubility in oils are generally less effective [64].

5 Conclusions

To establish a new class of OFMs, we assessed the friction and wear reduction performance of our synthesized C_{12}Amide-TEMPO, which is characterized by a TEMPO-based head group consisting of an amide linkage, a rigid six-membered ring, and a free oxygen radical terminal. In contrast to the conventional OFMs of GMO and stearic acid, whose friction coefficients increase with the normal load, the friction coefficient of C_{12}Amide-TEMPO remains at a low level even at the limit load of 43.7 N of the tribotester. Even compared with GMO and stearic acid at their effective load of 5.0 N, C_{12}Amide-TEMPO exhibits considerably more stable instantaneous friction coefficient and reduces the specific wear rate and surface roughness of wear tracks by more than 60%.

Moreover, we investigated the effect of the amide group by comparing C_{12}Amide-TEMPO with C_{12}Ester-TEMPO and C_{12}Amino-TEMPO for friction properties measured experimentally and molecular reactivity and surface adsorption properties calculated with the QM methods. The friction reduction effect of C_{12}Amide-TEMPO is far superior to those of C_{12}Ester-TEMPO and C_{12}Amino-TEMPO, highlighting the critical role of the amide group. We suggest from the QM calculation results that the boundary films formed by C_{12}Amide-TEMPO have a unique double-layer

structure. A strong surface adsorption layer is developed by the chemical interactions of the amide oxygen and free radical with iron oxide surfaces, and an upper layer is formed by the interlayer hydrogen-bonding between the amide hydrogen and free radical or the amide hydrogen and oxygen. Besides, the two types of hydrogen-bonding can form in each of the two layers. We suggest that the strong adsorption and interlayer and intralayer hydrogen-bonding enhance the strength of the boundary films to withstand long-time and heavily-loaded sliding, thereby leading to the high tribological performance of C_{12}Amide-TEMPO. The findings in this study are expected to provide new hints for future research on the molecular design of OFMs.

Acknowledgements

This work was supported in part by JSPS KAKENHI Grant (Nos. 19K21915 and 21H01238), JST Adaptable and Seamless Technology Transfer Program through Target-driven R&D (No. JPMJTM19FN), and NSK Foundation for Mechatronics Technology Advancement. We thank Dr. Kin-ichi OYAMA (Research Center for Materials Science, Nagoya University) for mass spectrometry analysis of the synthesized OFMs and associate professor Takayuki TOKOROYAMA (Graduate School of Engineering, Nagoya University) for the help with wear scar measurements. Jinchi HOU is grateful for the financial support from the China Scholarship Council (No. 202006030017).

Electronic Supplementary Material Supplementary material is available in the online version of this article at https://doi.org/10.1007/s40544-022-0610-0.

References

[1] Holmberg K, Erdemir A. Influence of tribology on global energy consumption, costs and emissions. *Friction* **5**(3): 263–284 (2017)

[2] Spikes H. Friction modifier additives. *Tribol Lett* **60**(1): 5 (2015)

[3] Tang Z L, Li S H. A review of recent developments of friction modifiers for liquid lubricants (2007–present). *Curr Opin Solid State Mater Sci* **18**(3): 119–139 (2014)

[4] Vaitkunaite G, Espejo C, Wang C, Thiébaut B, Charrin C, Neville A, Morina A. MoS_2 tribofilm distribution from low viscosity lubricants and its effect on friction. *Tribol Int* **151**: 106531 (2020)

[5] McQueen J S, Gao H, Black E D, Gangopadhyay A K, Jensen R K. Friction and wear of tribofilms formed by zinc dialkyl dithiophosphate antiwear additive in low viscosity engine oils. *Tribol Int* **38**(3): 289–297 (2005)

[6] Meng Y G, Xu J, Jin Z M, Prakash B, Hu Y Z. A review of recent advances in tribology. *Friction* **8**(2): 221–300 (2020)

[7] Zhou Y, Qu J. Ionic liquids as lubricant additives: A review. *ACS Appl Mater Interfaces* **9**(4): 3209–3222 (2017)

[8] Kenbeek D, Buenemann T, Rieffe H. Review of organic friction modifiers—Contribution to fuel efficiency? SAE Technical Paper, 2000: 2000-01–1792.

[9] Qiu S Q, Dong J X, Cheng G X. A review of ultrafine particles as antiwear additives and friction modifiers in lubricating oils. *Lubr Sci* **11**(3): 217–226 (1999)

[10] De Barros Bouchet M I, Martin J M, Avila J, Kano M, Yoshida K, Tsuruda T, Bai S D, Higuchi Y, Ozawa N, Kubo M, et al. Diamond-like carbon coating under oleic acid lubrication: Evidence for graphene oxide formation in superlow friction. *Sci Reports* **7**: 46394 (2017)

[11] Ewen J P, Gattinoni C, Morgan N, Spikes H A, Dini D. Nonequilibrium molecular dynamics simulations of organic friction modifiers adsorbed on iron oxide surfaces. *Langmuir* **32**(18): 4450–4463 (2016)

[12] Li W M, Kumara C, Meyer H M III, Luo H M, Qu J. Compatibility between various ionic liquids and an organic friction modifier as lubricant additives. *Langmuir* **34**(36): 10711–10720 (2018)

[13] Cyriac F, Yamashita N, Hirayama T, Yi T X, Poornachary S K, Chow P S. Mechanistic insights into the effect of structural factors on film formation and tribological performance of organic friction modifiers. *Tribol Int* **164**: 107243 (2021)

[14] Hirayama T, Kawamura R, Fujino K, Matsuoka T, Komiya H, Onishi H. Cross-sectional imaging of boundary lubrication layer formed by fatty acid by means of frequency-modulation atomic force microscopy. *Langmuir* **33**(40): 10492–10500 (2017)

[15] Wells H M, Southcombe J E. The theory and practice of lubrication: The '"Germ"' process. *J Soc Chem Ind* **39**(5): T51–T66 (1920)

[16] Deeley R M. Discussion on lubrication. *Proc Phys Soc London* **32**(1): 1s (1919)

[17] Guegan J, Southby M, Spikes H. Friction modifier additives, synergies and antagonisms. *Tribol Lett* **67**(3): 83 (2019)

[18] Ratoi M, Niste V B, Alghawel H, Suen Y F, Nelson K. The impact of organic friction modifiers on engine oil tribofilms. *RSC Adv* **4**(9): 4278–4285 (2014)

[19] Schwartz D K. Mechanisms and kinetics of self-assembled monolayer formation. *Annu Rev Phys Chem* **52**: 107–137 (2001)

[20] Beltzer M, Jahanmir S. Role of dispersion interactions between hydrocarbon chains in boundary lubrication. *A S L E Trans* **30**(1): 47–54 (1987)

[21] Jahanmir S. Chain length effects in boundary lubrication. *Wear* **102**(4): 331–349 (1985)

[22] Jahanmir S, Beltzer M. Effect of additive molecular structure on friction coefficient and adsorption. *J Tribol* **108**(1): 109–116 (1986)

[23] Okabe H, Masuko M, Sakurai K. Dynamic behavior of surface-adsorbed molecules under boundary lubrication. *A S L E Trans* **24**(4): 467–473 (1981)

[24] Campen S M. Fundamentals of organic friction modifier behaviour. Ph.D. Thesis. London (UK): Imperial College London, 2012.

[25] Zhang X W, Tsukamoto M, Zhang H D, Mitsuya Y, Itoh S, Fukuzawa K. Experimental study of application of molecules with a cyclic head group containing a free radical as organic friction modifiers. *J Adv Mech Des Syst Manuf* **14**(4): JAMDSM0044 (2020)

[26] Onumata Y, Zhao H Y, Wang C, Morina A, Neville A. Interactive effect between organic friction modifiers and additives on friction at metal pushing V-belt CVT components. *Tribol Trans* **61**(3): 474–481 (2018)

[27] Cyriac F, Tee X Y, Poornachary S K, Chow P S. Influence of structural factors on the tribological performance of organic friction modifiers. *Friction* **9**(2): 380–400 (2021)

[28] Fry B M, Moody G, Spikes H A, Wong J S S. Adsorption of organic friction modifier additives. *Langmuir* **36**(5): 1147–1155 (2020)

[29] Fry B M, Chui M Y, Moody G, Wong J S S. Interactions between organic friction modifier additives. *Tribol Int* **151**: 106438 (2020)

[30] Kano M, Yasuda Y, Okamoto Y, Mabuchi Y, Hamada T, Ueno T, Ye J, Konishi S, Takeshima S, Martin J M, et al. Ultralow friction of DLC in presence of glycerol mono-oleate (GNO). *Tribol Lett* **18**(2): 245–251 (2005)

[31] Kuwahara T, Romero P A, Makowski S, Weihnacht V, Moras G, Moseler M. Mechano-chemical decomposition of organic friction modifiers with multiple reactive centres induces superlubricity of ta-C. *Nat Commun* **10**: 151 (2019)

[32] Tatsumi G, Ratoi M, Shitara Y, Sakamoto K, Mellor B G. Effect of organic friction modifiers on lubrication of PEEK-steel contact. *Tribol Int* **151**: 106513 (2020)

[33] Nalam P C, Pham A, Castillo R V, Espinosa-Marzal R M. Adsorption behavior and nanotribology of amine-based friction modifiers on steel surfaces. *J Phys Chem C* **123**(22): 13672–13680 (2019)

[34] Hu W J, Xu Y H, Zeng X Q, Li J S. Alkyl-ethylene amines as effective organic friction modifiers for the boundary lubrication regime. *Langmuir* **36**(24): 6716–6727 (2020)

[35] Pominov A, Müller-Hillebrand J, Träg J, Zahn D. Interaction models and molecular simulation systems of steel–organic friction modifier interfaces. *Tribol Lett* **69**(1): 14 (2021)

[36] Desanker M, He X L, Lu J, Liu P Z, Pickens D B, Delferro M, Marks T J, Chung Y W, Wang Q J. Alkyl-cyclens as effective sulfur- and phosphorus-free friction modifiers for boundary lubrication. *ACS Appl Mater Interfaces* **9**(10): 9118–9125 (2017)

[37] Desanker M, He X L, Lu J, Johnson B A, Liu Z, Delferro M, Ren N, Lockwood F E, Greco A, Erdemir A, et al. High-performance heterocyclic friction modifiers for boundary lubrication. *Tribol Lett* **66**(1): 50 (2018)

[38] He X L, Lu J, Desanker M, Invergo A M, Lohr T L, Ren N, Lockwood F E, Marks T J, Chung Y W, Wang Q J. Boundary lubrication mechanisms for high-performance friction modifiers. *ACS Appl Mater Interfaces* **10**(46): 40203–40211 (2018)

[39] Cosimbescu L, Demas N G, Robinson J W, Erck R A. Friction- and wear-reducing properties of multifunctional small molecules. *ACS Appl Mater Interfaces* **10**(1): 1317–1323 (2018)

[40] Jaishankar A, Jusufi A, Vreeland J L, Deighton S, Pellettiere J, Schilowitz A M. Adsorption of stearic acid at the iron oxide/oil interface: Theory, experiments, and modeling. *Langmuir* **35**(6): 2033–2046 (2019)

[41] Li D M, Gao P, Sun X J, Zhang S W, Zhou F, Liu W M. The study of TEMPOs as additives in different lubrication oils for steel/steel contacts. *Tribol Int* **73**: 83–87 (2014)

[42] Prutton C F, Frey D R, Turnbull D, Dlouhy G. Corrosion of metals by organic acids in hydrocarbon solvents. *Ind Eng Chem* **37**(1): 90–100 (1945)

[43] Gallez B, Demeure R, Debuyst R, Leonard D, Dejehet F, Dumont P. Evaluation of nonionic nitroxyl lipids as potential organ-specific contrast agents for magnetic resonance imaging. *Magn Reson Imaging* **10**(3): 445–455 (1992)

[44] Nakatsuji S, Mizumoto M, Ikemoto H, Akutsu H, Yamada J I. Preparation and properties of organic radical compounds with mesogenic cores. *Eur J Org Chem* **2002**(12): 1912–1918 (2002)

[45] Waggoner A S, Keith A D, Griffith O H. Electron spin resonance of solubilized long-chain nitroxides. *J Phys Chem* **72**(12): 4129–4132 (1968)

[46] Li X, Deng X R, Kousaka H, Umehara N. Comparative study on effects of load and sliding distance on amorphous hydrogenated carbon (a-C:H) coating and tetrahedral amorphous carbon (ta-C) coating under base-oil lubrication condition. *Wear* **392–393**: 84–92 (2017)

[47] Liu X X, Yamaguchi R, Umehara N, Deng X R, Kousaka H, Murashima M. Clarification of high wear resistance mechanism of ta-CN_x coating under poly alpha-olefin (PAO) lubrication. *Tribol Int* **105**: 193–200 (2017)

[48] Frisch M J, Trucks G W, Schlegel H B, Scuseria G E, Robb M A, Cheeseman J R, et al. *Gaussian 16*, revision C.01. Wallingford CT (USA): Gaussian, Inc., 2016.

[49] Zhao Y, Truhlar D G. The M06 suite of density functionals for main group thermochemistry, thermochemical kinetics, noncovalent interactions, excited states, and transition elements: Two new functionals and systematic testing of four M06-class functionals and 12 other functionals. *Theor Chem Acc* **120**: 215–241 (2008)

[50] Ditchfield R, Hehre W J, Pople J A. Self-consistent molecular-orbital methods. IX. An extended Gaussian-type basis for molecular-orbital studies of organic molecules. *J Chem Phys* **54**(2): 724–728 (1971)

[51] Hariharan P C, Pople J A. The influence of polarization functions on molecular orbital hydrogenation energies. *Theor Chimica Acta* **28**(3): 213–222 (1973)

[52] Hehre W J, Ditchfield R, Pople J A. Self-consistent molecular orbital methods. XII. Further extensions of Gaussian-type basis sets for use in molecular orbital studies of organic molecules. *J Chem Phys* **56**(5): 2257–2261 (1972)

[53] Gattinoni C, Ewen J P, Dini D. Adsorption of surfactants on α-Fe_2O_3(0001): A density functional theory study. *J Phys Chem C* **122**(36): 20817–20826 (2018)

[54] Finger L W, Hazen R M. Crystal structure and isothermal compression of Fe_2O_3, Cr_2O_3, and V_2O_3 to 50 kbars. *J Appl Phys* **51**(10): 5362–5367 (1980)

[55] Dudarev S L, Botton G A, Savrasov S Y, Humphreys C J, Sutton A P. Electron-energy-loss spectra and the structural stability of nickel oxide: An LSDA+U study. *Phys Rev B* **57**(3): 1505–1509 (1998)

[56] Al-Kuhaili M F, Saleem M, Durrani S M A. Optical properties of iron oxide (α-Fe_2O_3) thin films deposited by the reactive evaporation of iron. *J Alloys Compd* **521**: 178–182 (2012)

[57] Klimeš J, Bowler D R, Michaelides A. Van der Waals density functionals applied to solids. *Phys Rev B* **83**(19): 195131 (2011)

[58] Fry B M, Moody G, Spikes H, Wong J S S. Effect of surface cleaning on performance of organic friction modifiers. *Tribol Trans* **63**(2): 305–313 (2020)

[59] Lu T, Chen F W. Multiwfn: A multifunctional wavefunction analyzer. *J Comput Chem* **33**(5): 580–592 (2012)

[60] Lu T, Chen F W. Quantitative analysis of molecular surface based on improved Marching Tetrahedra algorithm. *J Mol Graph Model* **38**: 314–323 (2012)

[61] Humphrey W, Dalke A, Schulten K. VMD: Visual molecular dynamics. *J Mol Graph* **14**(1): 33–38 (1996)

[62] Maslen E N, Streltsov V A, Streltsova N R, Ishizawa N. Synchrotron X-ray study of the electron density in α-Fe_2O_3. *Acta Crystallogr Sect B* **50**(4): 435–441 (1994)

[63] Momma K, Izumi F. VESTA 3 for three-dimensional visualization of crystal, volumetric and morphology data. *J Appl Crystallogr* **44**(6): 1272–1276 (2011)

[64] Minami I, Mori S. Concept of molecular design towards additive technology for advanced lubricants. *Lubr Sci* **19**(2): 127–149 (2007)

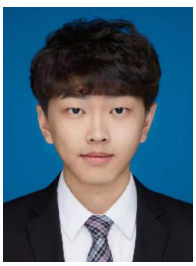

Jinchi HOU. He received his M.S. degree in power engineering and engineering thermophysics in 2020 from Beijing Institute of Technology, Beijng, China. He is currently a Ph.D. student at the Graduate School of Informatics, Nagoya University, Japan. His research interests focus on the applications of organic friction modifiers in nano-lubrication.

Masaki TSUKAMOTO. He received his M.S. and Ph.D. degrees in chemistry from Nagoya University, Japna, in 1994 and 1999, respectively. After working as a postdoctoral fellow at Université Paris-Sud, France, he joined the Graduate School of Information Science, Nagoya University from 2003. His current position is the lecturer at the Graduate School of Informatics, Nagoya University. His research interests include chemical synthesis of biologically relevant compounds, polymers, and organic friction modifiers.

Seanghai HOR. He received his M.S. degree in chemistry from Royal University of Phnom Penh, Cambodia, in 2015. He was an M.Ed. student at Aichi University of Education, Japan, from 2017 to 2019. He has recently earned his Ph.D. degree in informatics at Nagoya University, Japan. His current position is a teacher trainer at National Institute of Education, Cambodia. His research interests cover the organic and polymer synthesis.

Xingyu CHEN. He received his M.S. degree in vehicle operation engineering in 2019 from Beijing Jiaotong University, Beijing, China. He is currently a Ph.D. student at the Graduate School of Informatics, Nagoya University, Japan. His research interests focus on molecular orientation and chemical reaction in nano-lubrication, and multiscale computational simulations.

Juntao YANG. He received his B.E. degree in mechanical design and manufacturing and its automation from Guangdong University of Technology, China, in 2018. Then he pursed graduate studies at Nagoya University, Japan and received his M.S. degree in informatics in 2022. His research interests include molecular simulation, quantum mechanics calculation, machine learning, and tribological phenomena.

Hedong ZHANG. She received her B.E. degree in optical technique and photo-electric instrumentation from Zhejiang University, China, in 1994, and Ph.D. degree in electronic-mechanical engineering from Nagoya University, Japan, in 2002. Since then, she has been a member of the faculty at Nagoya University. She is currently a professor at the Graduate School of Informatics, Nagoya University. Her research interests include molecular simulation techniques, material informatics, and measurement techniques at the nanoscale, particularly for applications in the field of tribology.

Nobuaki KOGA. He received his Ph.D. degree in engineering from Kyoto University, Japan, in 1987. He was a research associate at the Institute for Molecular Science from 1986 to 1993 and an associate professor at Nagoya University, Japan, from 1993 to 1998. Since 1998, he has been a professor at Nagoya University. His research interests include chemical reactivity and excited state properties of organic and organometallic compounds.

Koji YASUDA. He received his M.S. and Ph.D. degrees in engineering from Kyoto University, Japan, in 1994 and 1997 respectively. He joined the Graduate School of Information Science at Nagoya University, Japan, from 1997. His current position is an associate professor. His research areas cover the quantum chemistry, solid state physics, and cheminformatics.

Kenji FUKUZAWA. He received M. Eng. in 1987 and Dr. Eng. in applied physics in 1997 from Nagoya University, Japan. He joined Nippon Telegraph and Telephone Corporation, Japan, in 1987 and was employed as a senior research engineer until 2000. He is currently a professor of the Department of Micro-Nano Mechanical Science and Engineering, Nagoya University. His research interests are micro/nano mechanical device engineering, nano-tribology, and their related measurement science and technology.

Shintaro ITOH. He received his Ph.D. degree in electromechanical engineering from Nagoya University, Japan, in 2006. Presently he is an associate professor at the Department of Micro-Nano Mechanical Science and Engineering, Nagoya University. His research areas are nano-metrology, nano-tribology, nano-rheology, and nano-fluidics. Especially his research interests include various kinds of solid–liquid interfacial phenomena ranging from confined liquid between solid surfaces to molecularly thin liquid films on solid surfaces.

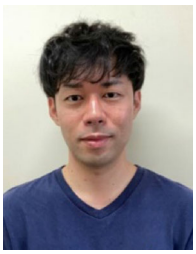

Naoki AZUMA. He received his M.S. and Ph.D. degrees in mechanical engineering from Nagoya University, Japan, in 2016 and 2018 respectively. His current position is an assistant professor at the department of Micro-Nano Mechanical Science and Engineering, Nagoya University. His research interests include micro-nano metrology, bioanalysis, micro-fluidic device, and micro-nano tribology.